

FE modelling of the Streicker Footbridge

*Original*

FE modelling of the Streicker Footbridge / Mulas, Maria Gabriella; Glisic, Branko; Domaneschi, Marco; Venuti, Fiammetta. - ELETTRONICO. - (2021), pp. 3229-3236. (Intervento presentato al convegno Proceedings of the Tenth International Conference on Bridge Maintenance, Safety and Management, IABMAS 2020 tenutosi a Sapporo, Japan nel 11 April 2021 through 15 April 2021) [10.1201/9780429279119-438].

*Availability:*

This version is available at: 11583/2914822 since: 2021-11-28T01:45:42Z

*Publisher:*

CRC Press

*Published*

DOI:10.1201/9780429279119-438

*Terms of use:*

This article is made available under terms and conditions as specified in the corresponding bibliographic description in the repository

*Publisher copyright*

Taylor and Francis postprint/Author's Accepted Manuscript (book chapters)

(Article begins on next page)

# FE modelling of the Streicker footbridge

M.G. Mulas

*Politecnico di Milano, Department of Civil and Environmental Engineering, Milan, Italy*

B. Glisic

*Princeton University, Department of Civil and Environmental Engineering, Princeton NJ, USA*

M. Domaneschi

*Politecnico di Torino, Department of Structural, Geotechnical and Building Engineering, Turin, Italy*

F. Venuti

*Politecnico di Torino, Department of Architecture and Design, Turin, Italy*

**ABSTRACT:** The Streicker footbridge was completed in 2010 at the Princeton University Campus, over the Washington Road. It is about 104 m long and consists of a central main span supported by a steel arch and four lateral approaching legs. The deck is a post-tensioned high-performance concrete girder. Steel columns with “Y” shape support four lateral legs that connect the bridge to the lateral bearings on the ground and the whole system results a slender varying cross section main girder. The original shape in the horizontal plane provides horizontal stability to the footbridge despite the intrinsic slenderness of the steel supporting columns. Vertical stability is provided also by the arch in the central main-span and by the supporting columns under the legs. Cross section width increases from the midpoint of the main span to the connections with the legs and then remains constant up to the ground bearings. This work is focused on the development of a finite element analysis of the footbridge at different levels of refinement from the essential implementation of beam elements to more refined FE solutions for the prestressed concrete deck. The models are identified with respect to the available operational modal parameters. This deck discretization could further allow simulating the motion of a running/walking pedestrian along different trajectories.

## 1 INTRODUCTION

Structural health monitoring (SHM) aims to assess condition and performance of the monitored structure. Several parameters can be monitored such as strain, acceleration, deflection, corrosion, etc., depending mostly on the monitoring aims, expected unusual behaviors (expected types of damage and deterioration), and available resources.

Design of structures is typically performed based on codes that impose certain safety and serviceability criteria, which are frequently given in terms of stresses and deflections. However, there are no practical SHM systems that can be deployed in long terms and in real-life settings to monitor directly these two parameters. Exceptions exist, but they are rather application specific. However, strain is parameter that is correlated to both stress and deflection and there is large variety of strain sensors that can be applied to virtually any type of real-life structure in long terms. These are the reasons why strain is frequently chosen in SHM applications.

An important step in SHM process is comparison of SHM outcomes with analytical and/or numerical models that are assumed to represent accurately the behavior of the structure. However, accurate modeling of the structure can be challenging due to complex geometrical shape of the structure and complex

interactions between materials forming the structure. Consequently, detailed modelling of entire structure might be impractical. Nevertheless, oversimplifying the model of the structure might result in important errors in predicted structural behavior.

Streicker Bridge on Princeton University campus is an example of structure, which features complexity in shape and materials. The conceptual design of the bridge was made by Christian Menn (1927-2018), while detailed design was performed by Theodore P. Zoli and Ryan Woodward of HNTB. The bridge combines deck stiffened arch with four diverging curved continuous girders and prestressed high-performance concrete with weathering steel. The bridge strikes by its elegance, slenderness and effective use of shape for both structural and aesthetic purposes. During construction, in 2009, the bridge was instrumented by fiber-optic strain and temperature sensors (Hubbel & Glisic 2013).

The broader aim of this study is to create moderately simplified numerical models of complex structure and evaluate their performance when used in strain-based SHM. The scope of the project is limited to dynamic structural identification, while other aspects such as evaluation of stresses, deflections, and unusual structural behaviors, will be explored in future work. Streicker Bridge is used as the case study of the project.

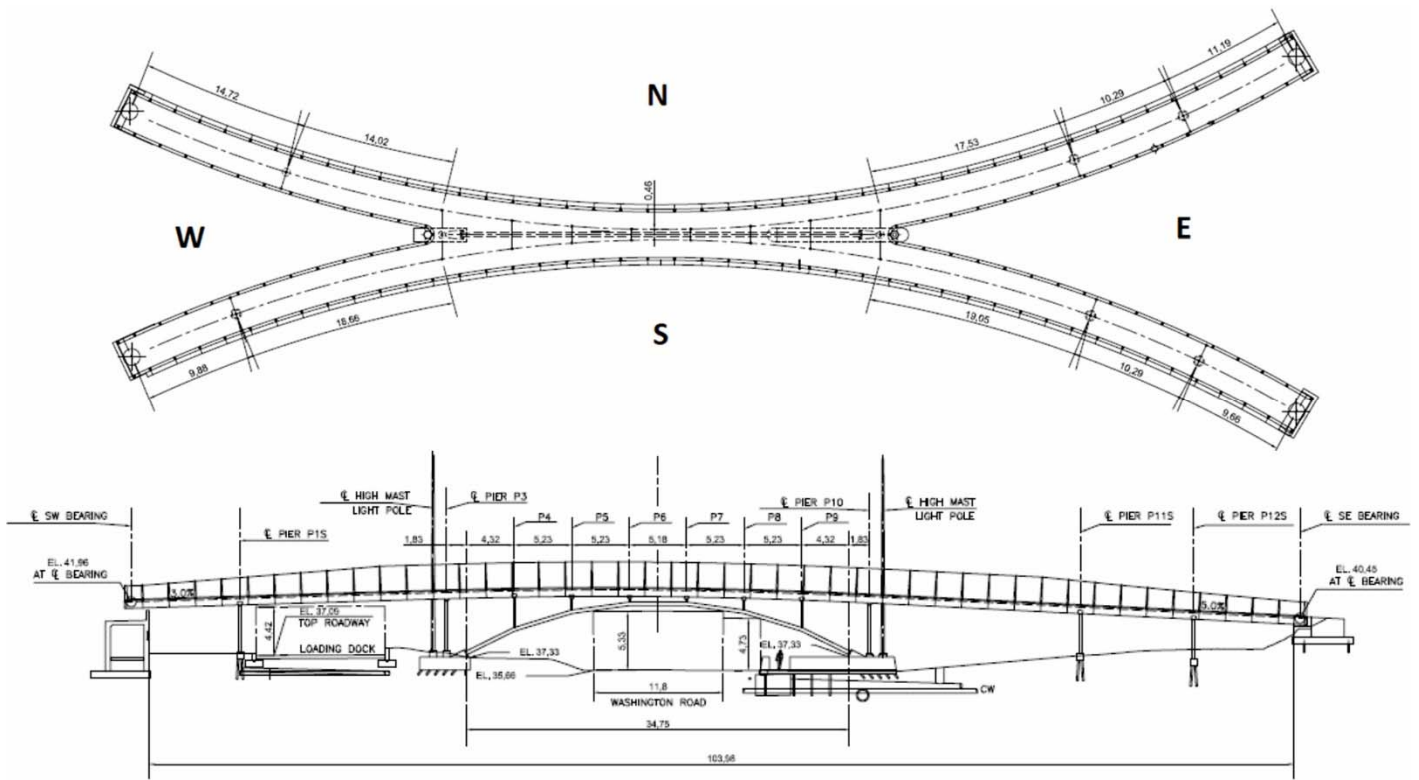


Figure 1. Plan and elevation view (image credit: Princeton University Facilities and HNTB)

## 2 DESCRIPTION OF THE FOOTBRIDGE

The Streicker footbridge is located at the Princeton University Campus (New Jersey, USA) and connects the western to the eastern part of the campus. It is a 104m-long structure and consists of a main span, (deck stiffened arch) and four lateral approaching legs (continuous curved girders), see Fig. 1. In plan, the footbridge geometry results from two intersecting arches that assure lateral stability to the steel arch supporting the main span.

section is constant in the four legs and variable in the main span, with maximum width in the sections where the legs join the main span.

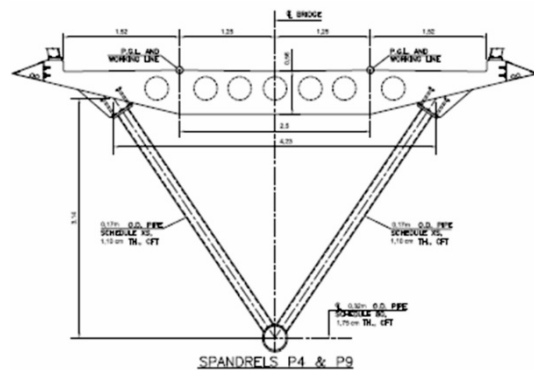


Figure 3. Detail of one spandrel (PU Facilities & HNTB)

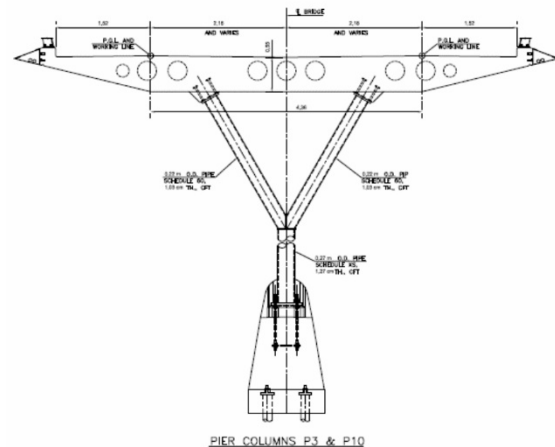


Figure 2. Detail of one Y-shaped pier (PU Facilities & HNTB)

The deck, made of post-tensioned high-performance concrete, is connected through six spandrels to the steel arch in the main span and is supported by eight Y-shaped piers along the lateral legs (Fig. 2-3). Both main arch, spandrels and piers are made of weathering steel tubes filled with self-consolidating concrete. The depth of the deck is 578 mm and the diameter of the tubular arch beams is 324 mm. The deck cross

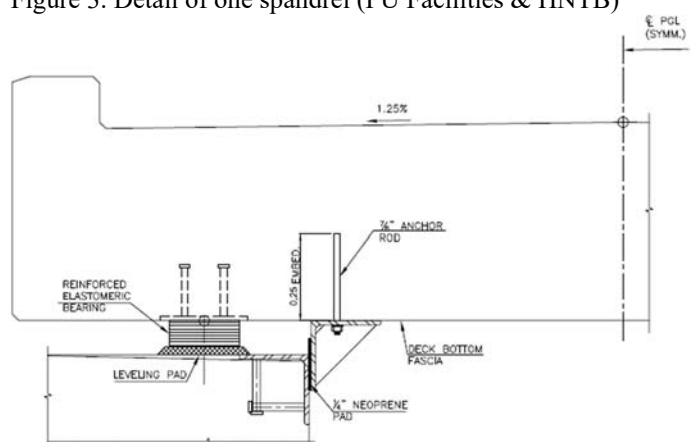


Figure 4. West abutment bearing detail (PU Facilities & HNTB)

At the abutments, the deck rests on elastomeric neoprene bearings (Fig. 4). Both piers and arch are fixed

to concrete footings, which are supported on micropiles (Fig. 5). The deck is connected to the piers and spandrels through fixed connections.

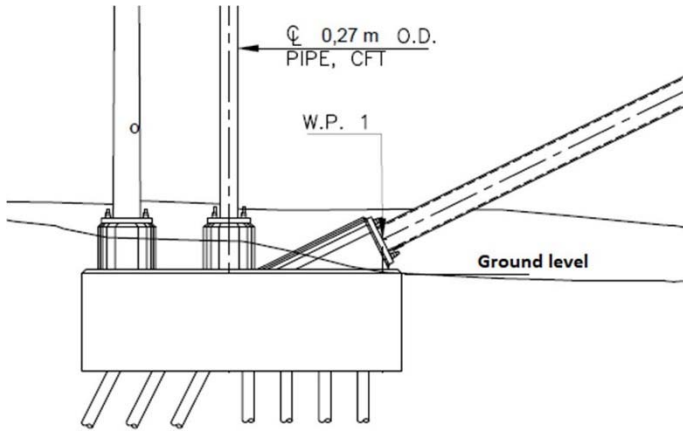


Figure 5. West footing of the arch and pier P3 (PU Facilities & HNTB)

## 2.1 Materials

The concrete mixture for the deck was designed to meet the New Jersey Department of Transportation (NJDOT) specifications for Class A High-Performance Concrete (HPC). The 28-day compressive strength from cylinder tests was 51 and 59 MPa for the main span and the legs, respectively. The Young's modulus was 37.5 GPa (Sigurdardottir & Glisic 2015).

Arch, piers and spandrels are made of round hollow structural steel (HSS) with minimum yield strength of 345 MPa and minimum ultimate strength of 483 MPa, in conformity to ASTM A847-05. All pipes are designated as CFT (concrete filled tubes).

## 2.2 Design loads

The dead loads adopted in design are reported in Table 1. The pedestrian live load, defined according to AASHTO (Guide Specifications for Design of Pedestrian Bridges, section 1.2), equals 31.11 kN/m<sup>2</sup>. The design wind loads were assumed to be 3.59 kN/m<sup>2</sup>, applied on the vertical projected area perpendicular to the longitudinal axis for arch structures.

## 2.3 Monitoring system

The Streicker bridge is equipped with two fiber-optic-based monitoring systems embedded in the concrete deck (Sigurdardottir & Glisic 2015): a system for global structural monitoring based on discrete fiber Bragg-grating (FBG) long-gauge strain and temperature sensors and a Brillouin-scattering based distributed sensing system for integrity monitoring. Since the bridge is almost symmetrical in plan, the sensors were installed on half the main span and on the longest leg (southeast leg). Only the FBG system is relevant for this research work due to its capability for dynamic monitoring.

Table 1. Design dead loads

Reinforced concrete [kN/m <sup>3</sup> ]	23.56
Post-tensioned concrete [kN/m <sup>3</sup> ]	24.35
Lightweight concrete [kN/m <sup>3</sup> ]	18.06
Structural steel [kN/m <sup>3</sup> ]	76.97
Bridge railings [kN/m]	0.730
Utilities [kN/m]	0.219
Future wearing surface [kN/m <sup>2</sup> ]	0.718

## 3 NUMERICAL MODELLING

The peculiar geometry of the footbridge, with a main span “splitting” in two legs at each side, raises the problem of modelling the zones of transition between the central span and the legs. For this reason, two different FE models have been built in ANSYS Mechanical APDL:

- Model *AnsysBeam* (*AB model*) that contains only beam elements: the transition zone is approximately taken into account through creating a rigid region that connects the eccentric axis lines of central span and legs.

- Model *AnsysShell* (*AS model*): the deck geometry in plan is reproduced correctly through shell elements.

In both models it is necessary to account for the variable geometry of the deck cross-section. The results of the two models allows for the evaluation of the sensitivity of modal properties to the transition zone modelling, also by comparison with the available experimental results. As it will be shown in the following, the two models share a set of assumptions and input data.

### 3.1 Modelling assumptions

Under the assumption of linear behavior of materials and perfect bond with tendons, the effect of the deck post-tensioning on the modal results was neglected, since the variations in the deformed equilibrium configuration do not modify significantly the dynamic properties of the structure (Breccolotti et al. 2009).

Since only a limited set of cross-section shapes for beam elements is available to the analyst, the variable geometry of the deck, made complex by the interior holes (see Figs. 2 and 3), cannot be accounted for directly in ANSYS. As an alternative, the tensor of moments of inertia can be provided in input. To have the same geometrical description both in the *AB* and in the *AS* model, five equivalent rectangular sections were adopted to represent the deck. The dimension  $b$  and  $h$  of the equivalent cross sections are chosen to match the moments of inertia of the real cross section ( $I_x = bh^3/12$ ,  $I_y = hb^3/12$ ). The effective area ( $A_{eff} = bh$ ) of the equivalent sections is larger than the real one ( $A_{real}$ ), due to the presence of the holes. Table 2 shows the dimensions of the equivalent sections, referring to

the pier names (from pier P3 to pier P10) shown in the elevation view (Fig. 1).

Table 2. Equivalent rectangular cross-sections of the concrete deck.

	P6&P7	P5&P8	P4&P9	P3&P10	Legs
$h$ [m]	0.52	0.53	0.55	0.56	0.48
$b$ [m]	3.68	4.15	5.05	6.70	3.20
$A_{eff}$ [m <sup>2</sup> ]	1.93	2.22	2.77	3.75	1.54
$A_{real}$ [m <sup>2</sup> ]	1.46	1.74	2.24	3.21	1.28
$I_x$ [m <sup>4</sup> ]	0.04	0.05	0.07	0.10	0.03
$I_y$ [m <sup>4</sup> ]	2.17	3.20	5.90	14.02	1.31

Due to the difference in the effective area of the deck cross-sections, a reduction of the density of the concrete was applied in order to preserve the total mass. Table 3 reports the implemented concrete properties. Similarly, the density of structural steel was modified to account for the concrete infilling.

Table 3. Concrete properties.

	P6-P7	P5-P8	P4-P9	P3-P10	Legs
$q$ [kg/m <sup>3</sup> ]	2070	2129	2173	2280	2269
$E_c$ [GPa]	35	35	35	35	36
$f_c$ [MPa]	41	41	41	41	41

In both models, the deck and the piers nodes at every pier/spandrel location are connected using rigid body constraints between the centroid of the deck and the two upper nodes of every Y-shaped pier or spandrel (three nodes in total). Thus, all degrees of freedom (6 DOF) are constrained, in accordance to the bolted connection between deck and pipes.

### 3.2 AnsysBeam (AB) model

For the AB model, the complex geometry of the foot-bridge was imported directly from a CAD file, while the nodes coordinates were exported from AutoCAD to Excel. Subsequently, the coordinates were written in a text format file following the rules of the ANSYS APDL software. The AB model contains 97 nodes and 83 Timoshenko beam elements (Figure 6) named BEAM188, having 6 dofs per node. The element can be used both for slender and stout beams. The deck elements were assigned the five equivalent rectangular cross-sections described in Table 2, depending on their position. Beam nodes do not have offset with respect to the mesh nodes that are located in the middle plane of the deck. In a similar way, the arch, piers and spandrels were modelled with four different pipe cross-sections based on their real dimensions, not reported here for the sake of brevity.

As it can be noticed in Figure 6, deck and piers nodes are not connected by any element. Thus, the body constraint CERIG was used. The command creates a rigid region by writing constraint equations to define rigid lines linking a designated retained (or "master") node to a number of removed (or "slave")

nodes. For the case at study, the retained node is the deck node at pier or spandrel locations and the removed nodes are the two upper nodes of every Y-shaped pier and spandrel. The six degrees of freedom (DOFs) of the removed nodes are all constrained in this way, and no independent equilibrium equation is written for them. The bases of the piers and of the arch are fixed, while the supports at the four abutments are simple supports where all the translations are constrained, while all the rotations are allowed. The model was preliminary validated by comparing the resultant of the vertical reactions due to self-weight (6902.50 kN) to the weight value computed manually (6904.72 kN).

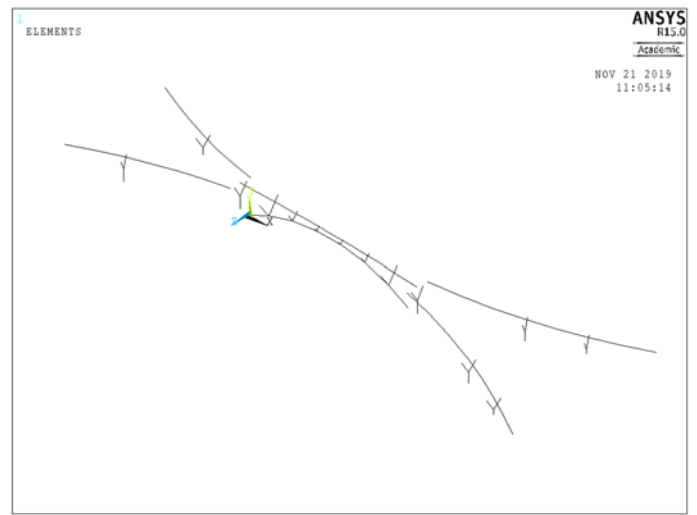


Figure 6. View of the AnsysBeam model

### 3.3 AnsysShell (AS) model

The nodes of the AS model presented in this Section have the same IDs of the AB model for the arch, piers and spandrels. Nevertheless, the deck nodes have a different numeration. The model, depicted in Figure 7, contains 515 nodes.

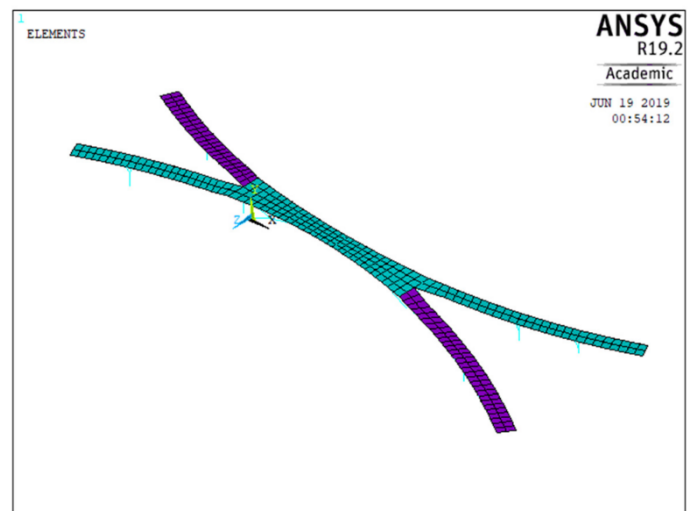


Figure 7. View of the AnsysShell model mesh.

Also in this model, the BEAM188 element was used for the arch, piers and spandrels. The deck is discretized with SHELL181 elements, a four-node element with six DOFs at each node: translations in the x, y, and z directions, and rotations about the x, y, and z-axes. This shell element is suitable for analyzing thin to moderately thick shell structures. In total, the AS model contains 367 elements: 43 beam elements to model the arch, piers and spandrels and 324 shell elements to model the deck (Figure 7).

The shell elements adopted for the deck are rectangular, having size of approximately 1×1 m. The elements nodes are created by a direct user-defined generation. In the four legs, two shell elements suffice to describe the deck cross-section. Conversely, four shell elements are necessary for the main span cross-section. Since the shell elements allow constructing a tapered deck, the variation of the cross-section in the main span of this model is smoother than in the AB model. Adjacent shell elements connect to each other at the mid-plane of the deck, so they do not have an offset.

In the same way as for AB model, arch, piers and spandrels adopt four different pipe cross-sections based on the real dimensions of the bridge. Differently from AB model, the deck is continuous between the legs and the main span. However, the deck and the piers nodes are not connected by any element. Therefore, at every pier or spandrel location, two constraint equations CERIG to constrain the six degrees of freedom are used: the two upper nodes of the pier or spandrel are constrained with their closest node of the deck shell, respectively. The boundary conditions are the same as in the AB model. The self-weight validation was positively performed also in this case.

## 4 RESULTS

To validate the FE models, the natural frequencies from modal analysis are compared to those experimentally determined (Sigurdardottir & Glisic 2015, Sabato 2015, Domaneschi et al. 2018). The frequencies identified in Sigurdardottir & Glisic (2015) and Domaneschi et al. (2018) are based on the embedded fiber optic sensor system that measures dynamic curvature in the vertical plane along the footbridge axis. Sabato (2015) adopted a conventional accelerometer.

Tests adopted different conditions of dynamic loading. In Sigurdardottir & Glisic (2015) frequencies were identified from three dynamic tests involving five people running over the deck of the southeast leg (P10-P11 span). In Sabato (2015) eight people were randomly running on the bridge. In Domaneschi et al. (2018) pedestrians (groups of Campus students) were randomly walking and running on the bridge at unknown frequencies. Table 4 reports the identified natural frequencies, related to South-East leg. Tests provided consistent values of the first two natural

frequencies. Small discrepancies among them can be justified by different environmental conditions. Since the mode shapes were not identified in tests, the comparison is made on natural frequencies only. Figure 8 shows a typical Power Spectral Density (PSD) of a representative dynamic test (Domaneschi et al. 2018). The Periodogram of the dynamic curvature in a vertical plane in Figure 8 is split into two parts: one in the range 2–4Hz (top of Fig. 8) and one in the range 4–8 Hz (bottom of Fig. 8). A different scale allows highlighting small intensities in the range 4–8 Hz.

Table 4. Natural frequencies from the literature [Hz].

Ref.	$f_1$	$f_2$	$f_3$	$f_4$	$f_5$	$f_6$
Sigurdardottir & Glisic	3.11	3.72				
Sabato	3.08	3.75				
Domaneschi et al.	3.00	3.65	4.46	4.95	6.02	7.81

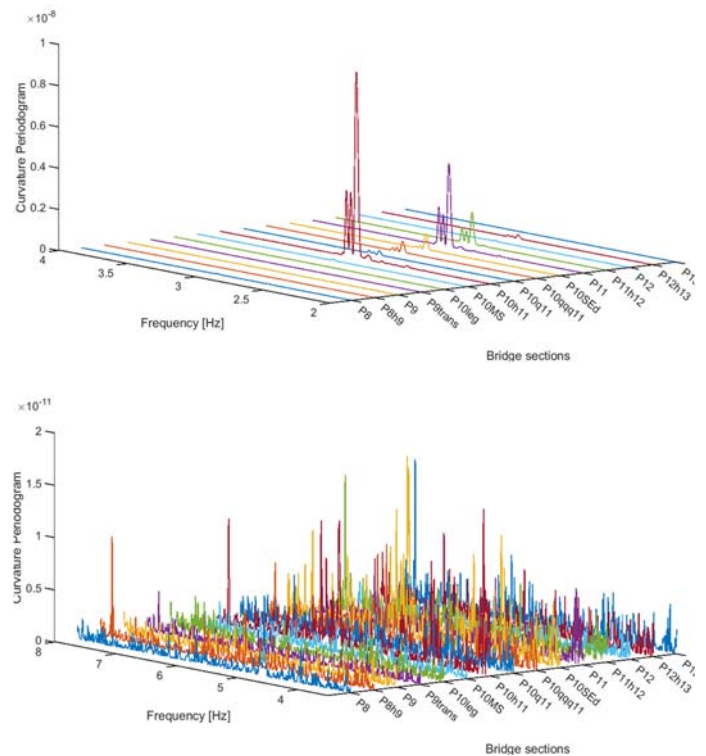


Figure 8. Periodogram PSD of dynamic curvature for a representative dynamic test (Domaneschi et al. 2018).

A numerical modal analysis on the two FE models provided the natural frequencies of the first 14 modes, contributing to about 85% and 77% of modal participating mass for AS model and AB model, respectively. Figs. 9 and 10 show the first five mode shapes and natural frequencies obtained for the AS and AB model, respectively. In each mode, the four legs undergo a different deformation. The tentative description of the dominant deflected shape in Figs. 9 and 10 refers to the southeast leg. For both models, the first mode shape appears to be the one related to the main arch, with a null point at mid-span, as expected. A significant torsional component is more apparent in the AS model where the deck is discretized with shell elements. All legs deforms in the first mode shape.

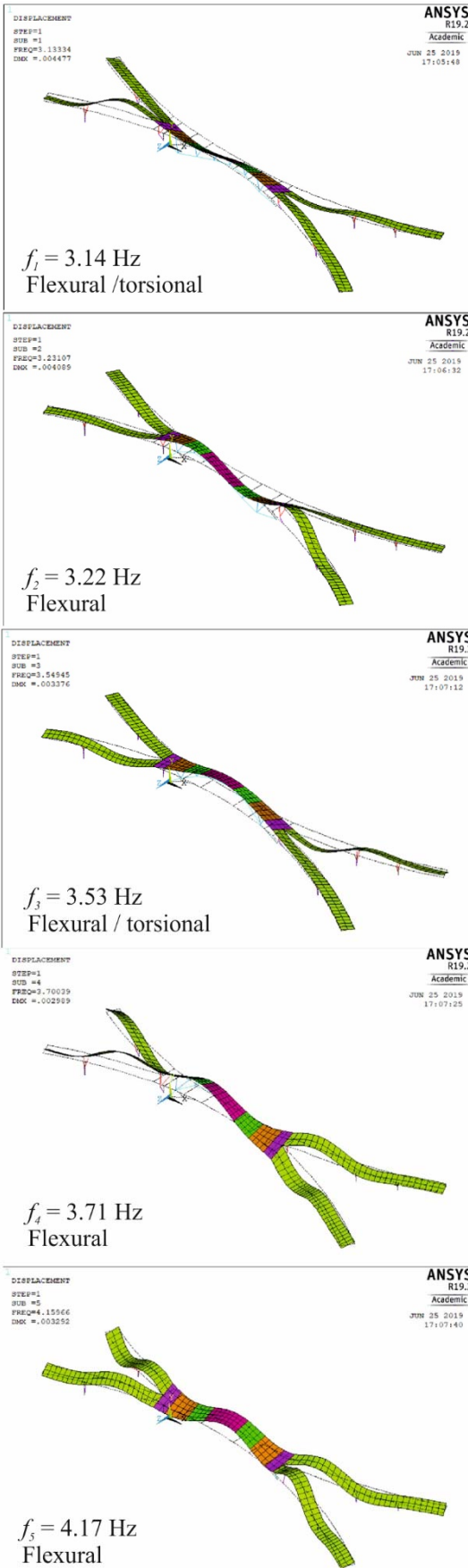


Figure 9. Mode shapes and frequencies from model AS

Table 5 shows the comparison between experimental and numerical frequencies. In all cases, there is an excellent match between the first numerical and experimental frequency. However, the second experimental frequency matches the fourth numerical one for both models. Relative errors  $\varepsilon$  are below 5%.

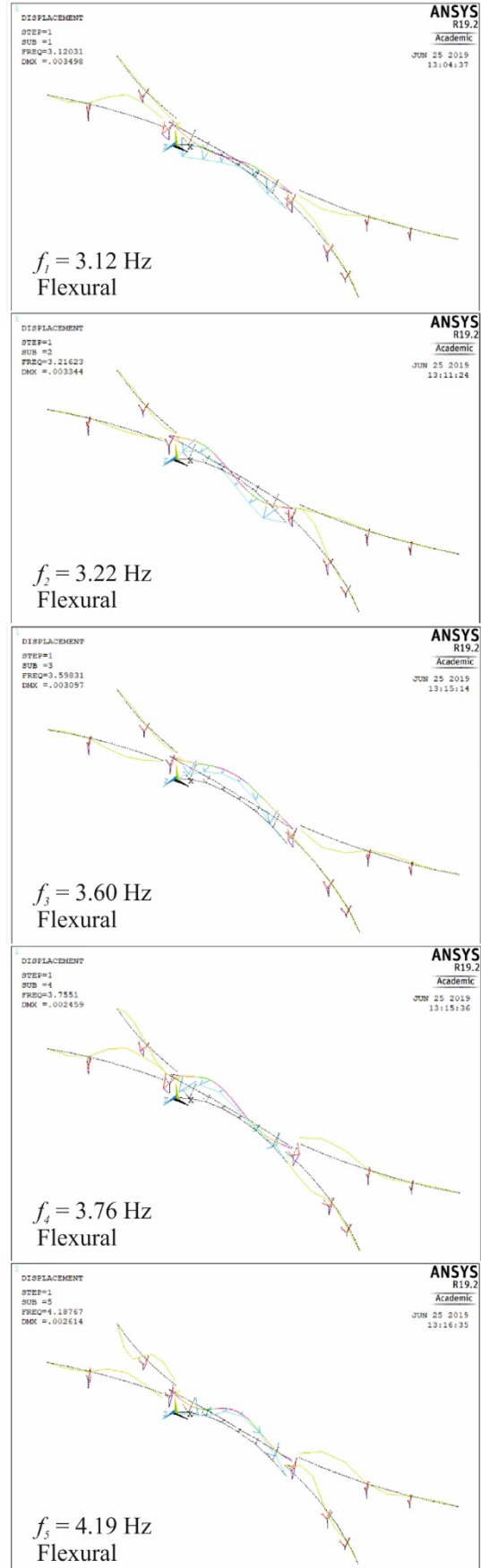


Figure 10. Mode shapes and frequencies from model AB

There can be several reasons for the discrepancy in the order of the modes. First of all, it must be kept in mind that sensors were located only in the Southeast leg and in part of the main span. Second, sensors were able to collect parallel strains in the vertical plane (along the bridge axis). Thus, they could not detect

physical modes straining different fibers, as lateral flexural modes. Third, in general a FE model, especially with a fine discretization as the AS model, can detect modes that are difficult to be identified with sensors, either because the level of excitation related to the mode is low or because they involve displacements in directions that are not recorded by sensors.

Table 5. Experimental vs numerical frequencies

$f_{exp}$ [Hz]	$f_{AB}$ [Hz]	$\varepsilon_{AB}$	$f_{AS}$ [Hz]	$\varepsilon_{AS}$
<i>Sigurdardottir</i>				
		[%]		[%]
3.11	3.12	0.32	3.14	0.96
3.72	3.76	1.07	3.71	-0.26
<i>Sabato</i>				
		[%]		[%]
3.08	3.12	1.02	3.14	1.90
3.75	3.76	0.26	3.71	-1.00
<i>Domaneschi</i>				
		[%]		[%]
3.00	3.12	4.00	3.14	4.66
3.65	3.76	3.01	3.71	1.64

In general, the behavior of the structure at study is not easily predictable. In fact, the bridge does not possess axes of symmetry and consists of five weakly interconnected parts. As a result, the legs may have different responses in the same mode shape. Participating masses could give an index of “activation” of a single part in each mode, but ANSYS provides only global values, without distinguishing the contribution of different parts in different directions (i.e. horizontal or vertical). Thus, it comes as no surprise that, for the second and third mode, only the numerical mode is detected but not its experimental counterpart.

Table 6. MAC values between models AB and AS

		Model AB						
		1	2	3	4	5	6	7
Model AS	1	<b>0.83</b>	0.00					
	2	0.46	<b>0.86</b>	0.01				
	3		0.04	<b>1.00</b>	0.12			
	4			0.15	<b>0.99</b>	0.02		
	5				0.01	<b>0.99</b>	0.49	
	6					0.01	0.09	<b>0.98</b>
	7						0.36	0.22

Finally, it is important to verify the consistency of the results of the two FE models in terms of modal properties. The natural frequencies in Figures 9 and 10 show an excellent agreement. A visual comparison shows a good agreement also in terms of modal shapes. From the numerical point of view, the Modal Assurance Criterion (MAC) (Allemang & Brown 1983) is adopted to verify the correlation between the mode shapes extracted from the two FE models. The MAC index is computed considering vertical displacements at the same nodes. Table 6 lists the values related to the first seven modes: the first five modes

are strongly correlated, with MAC values higher than 0.83, while a low correlation is found for modes 6 and 7. From the MAC values, it could be argued that the 6<sup>th</sup> mode of the AS model coincides with the 7<sup>th</sup> mode of the AB model.

## 5 CONCLUSIONS

In this work two FE models of the Streicker foot-bridge at the Princeton University Campus were developed. The models differ in the deck modelling: the simpler AB model adopts only beam elements, while in the more complete AS model the deck is discretized with shell elements. The models are validated by comparing their natural frequencies with the ones identified experimentally in three different dynamic tests from the literature. The results of the two FE models are in good agreement in terms of both natural frequencies and mode shapes. A comprehensive comparison with experimental modal properties was not possible due to the lack of experimental mode shapes. The comparison of natural frequencies showed an excellent agreement in terms of the first natural frequency. The second experimental frequency matches the frequency of the fourth numerical mode, a discrepancy that has been justified in the paper.

Based on “quasi-symmetry” considerations, strain sensors were located only on the Southeast leg and in the southern side of the half mid-span. Conversely, it is difficult to identify in the numerical analysis the role of this leg: even though the bridge geometry shows that the main span and the four legs are only weakly interconnected, a dynamic interaction takes place anyway. From the numerical point of view, the role played by the main span on each leg could be found by a sub-structuring approach, based on frequency domain analysis. On the experimental side, ambient vibration tests (AVTs) could be performed, adopting a sufficient number of conventional accelerometers. A carefully designed layout of these devices on the whole bridge, guided by the preliminary results of the AS model and measuring both horizontal and vertical acceleration, could provide the experimental mode shapes and the sought contributions of the southeast leg to the global dynamic behavior.

The good and similar performances of the proposed FE models do not allow identifying one of the two as the best one. The choice of the model to be adopted in subsequent analyses should be dictated by the aim to be pursued. The AS model contains a fine meshing of the deck. This feature allows for the numerical study of dynamic interaction with mechanical systems moving on the bridge along eccentric trajectories. Thus, the outcome of previous experimental tests on the bridge, involving either a heavy vehicle or running/walking pedestrians, could be numerically simulated. More important, the FE model provides an

excellent tool for fully exploiting the richness of the data provided by the SHM sensors net on the bridge.

#### ACKNOWLEDGEMENTS

Dorotea Sigurdardottir, Jose Pedro Sousa Afonso, David Hubbell, Kaitlyn Kliever, Yao Yao, Jack Reilly, and Hiba Abdel-Jaber performed various tests on the Streicker Bridge. Marc Lizana (PoliMI) and Umberto Verardo (PoliTO) analyzed the footbridge for their MS thesis in Civil Engineering. Their contribution is gratefully acknowledged.

#### REFERENCES

- Abdel-Jaber, H & Glisic, B. 2014. A method for the on-site determination of prestressing forces using long-gauge fiber optic strain sensors. *Smart Mater. Struct* 23: 075004
- Allemang, R.J. & Brown, D.L. Correlation coefficient for modal vector analysis. In: *Proceedings of the 1st Int. Modal Analysis Conf. (IMAC-I)*, Orlando, FL, USA, 1983.
- ANSYS, Online Manuals Release 5.5, 2015.  
[http://mostreal.sk/html/guide\\_55/GBooktoc.html](http://mostreal.sk/html/guide_55/GBooktoc.html).
- Breccolotti, M., Ubertini, F., & Venanzi, I. 2009. Natural frequencies of prestressed concrete beams: theoretical prediction and numerical validation. In *Proceeding of the XIX Aimeta Conference*, Ancona, Italy, 2009.
- Domaneschi, M., Cimellaro, G.P., Apostoliti, C., Glisic, B., & Kliewer, K. 2018. Monitoring Footbridges Using Wireless Mesh Networks, *9th International Conference on Bridge Maintenance, Safety and Management (IABMAS 2018)*, Melbourne, Australia, 9-13 July 2018.
- Hubbel, D. & Glisic, B. 2013. Detection and Characterization of Early-Age Thermal Cracks in High-Performance Concrete. *ACI Materials Journal* 110(M28):323-330.
- Sabato, A. 2015. Pedestrian bridge vibration monitoring using a wireless MEMS accelerometer board, *IEEE 19th International Conference on Computer Supported Cooperative Work in Design (CSCWD)*, Calabria I.
- Sigurdardottis, D.H & Glisic, B. 2015. On-site validation of fiber-optic methods for structural health monitoring: Streicker Bridge. *J Civil Struct Health Monit* 5: 529-549.